Explicit Runge-Kutta Method for Unsteady Rotor/Stator Interaction

Philip C. E. Jorgenson* and Rodrick V. Chima*
NASA Lewis Research Center, Cleveland, Ohio

A quasi-three-dimensional rotor/stator analysis has been developed for blade-to-blade flows in turbomachinery. The analysis solves the unsteady Euler or thin-layer Navier-Stokes equations in a body-fitted coordinate system. It accounts for the effects of rotation, radius change, and stream surface thickness. The Baldwin-Lomax eddy-viscosity model is used for turbulent flows. The equations are integrated in time using a four-stage Runge-Kutta scheme with a constant time step. Results are shown for the first stage of the Space Shuttle main engine high-pressure fuel turbopump. Euler and Navier-Stokes results are compared on the scaled single- and multipassage machine. The method is relatively fast, and the quasi-three-dimensional formulation is applicable to a wide range of turbomachinery geometries.

Introduction

THE major thrust of the computational analysis of turbomachinery to date has been the steady-state solution of isolated blades using mass-averaged inlet and exit conditions. Unsteady flows differ from the steady solution due to interaction of pressure waves and wakes between blade rows. To predict the actual complex flow conditions, one must look at the time-accurate solution of the entire turbomachine.

Supersonic computations have been made by Rai[1] of unsteady flow in a rotor/stator configuration. Rai[2] also computed a subsonic flow case of a turbine stator using an implicit scheme. He used overlaid O- and H-grids around the blade with a conservative treatment at the interface. Gibeling et al.[3] have used an implicit scheme with a distorting grid at the interface. Oden and Bass[4] used a finite-element scheme with an explicit Lax-Wendroff time-marching algorithm, along with adaptive mesh refinement to solve Rai's supersonic model problem. Giles[5] solves the unsteady inviscid Euler equations using an explicit Lax-Wendroff algorithm. A technique is used that inclines the computational plane in time such that flows can be computed in turbomachines with an arbitrary stator/rotor pitch ratio. Three-dimensional solutions have been reported by Rai.[6] Here, the unsteady, thin-layer Navier-Stokes equations are solved using a third-order-accurate, implicit, upwind scheme. The solution procedure solves for flow in axial-flow turbomachinery with equal stator/rotor blade ratios.

Many of the numerical tools used in the analysis of isolated blades can be used for time-accurate rotor/stator interaction analysis. Here, the quasi-three-dimensional Euler or thin-layer Navier-Stokes equations are solved on body-fitted C-grids. An explicit four-stage Runge-Kutta algorithm is used with a constant time step. Computer time is reduced by vectorization. Most turbomachinery analyses assume periodicity from blade to blade. This makes it possible to analyze one blade only. Turbomachinery is designed with unequal number of blades to avoid forced vibration problems. Therefore, a full unsteady analysis must include at least a few passages on each wheel.

Presented as Paper 88-0049 at the AIAA 26th Aerospace Sciences Meeting, Reno, NV, Jan. 11-14, 1988; received May 10, 1988; revision received Aug. 8, 1988.

*Aerospace Engineer. Member AIAA.

The numerical method is presented as well as viscous results for the first stage of the Space Shuttle main engine (SSME) high-pressure turbopump. Comparisons are made between a scaled 1:1 and 2:3 stator/rotor blade configurations of the turbopump. Inviscid results are computed for comparison on the 1:1 stator/rotor configuration.

Governing Equations

The axisymmetric (m, θ) coordinate system used for the quasi-three-dimensional analysis is shown in Fig. 1. Here the m coordinate is defined by

$$(\mathrm{d}m)^2 = (\mathrm{d}z)^2 + (\mathrm{d}r)^2 \tag{1}$$

and the θ coordinate is defined by

$$\theta = \theta' - \Omega t \tag{2}$$

where θ' is fixed in space and θ rotates with the blade row with angular velocity Ω. The radius r and the stream surface thickness h are taken to be known functions of m.

The flow equations are written in the (m, θ) system[7,8] and then are transformed to a general body-fitted (ξ, η) system using standard methods. The thin-layer approximation is used to eliminate all viscous derivatives in the streamwise ξ direc-

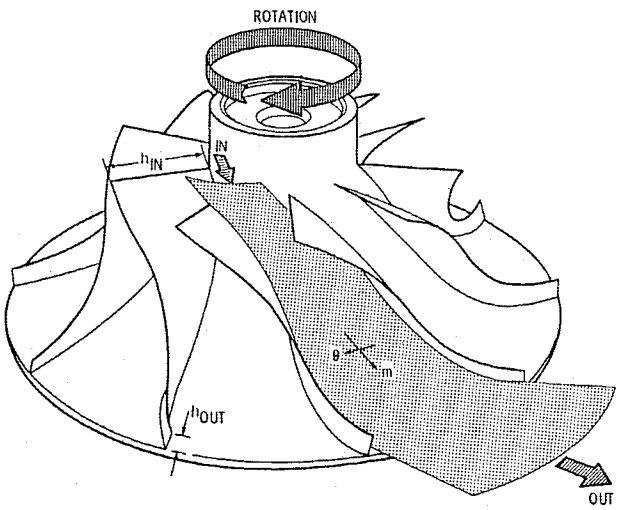

Fig. 1 Quasi-three-dimensional stream surface and coordinate system for a centrifugal compressor.

tion. The final equations are

$$\partial_t \hat{q} + \partial_\xi \hat{F} + \partial_\eta (\hat{G} - Re^{-1}\hat{S}) = \hat{K} \tag{3}$$

The inviscid flux terms are given by

$$\hat{q} = \bar{J}^{-1}\begin{bmatrix} \rho \\ \rho v_m \\ \rho v_\theta r \\ e \end{bmatrix}, \quad \hat{F} = \bar{J}^{-1}\begin{bmatrix} \rho W^\xi \\ \rho v_m W^\xi + \xi_m p \\ (\rho v_\theta W^\xi + \bar{\xi}_\theta p)r \\ (e+p)W^\xi + \bar{\xi}_\theta r \Omega p \end{bmatrix}$$

$$\hat{K} = \bar{J}^{-1}\begin{bmatrix} 0 \\ K_2 \\ 0 \\ 0 \end{bmatrix}, \quad \hat{G} = \bar{J}^{-1}\begin{bmatrix} \rho W^\eta \\ \rho v_m W^\eta + \eta_m p \\ (\rho v_\theta W^\eta + \bar{\eta}_\theta p)r \\ (e+p)W^\eta + \bar{\eta}_\theta r \Omega p \end{bmatrix} \tag{4}$$

The relative contravariant velocity components W^ξ and W^η along the ξ and η grid lines are given by

$$W^\xi = \xi_m v_m + \bar{\xi}_\theta w_\theta, \quad W^\eta = \eta_m v_m + \bar{\eta}_\theta w_\theta \tag{5}$$

where $w_\theta = v_\theta - r\Omega$ is the relative tangential velocity component. The energy and pressure are given by

$$e = \rho[C_v T + \tfrac{1}{2}(v_m^2 + v_\theta^2)] \tag{6}$$

$$p = (\gamma - 1)[e - \tfrac{1}{2}(v_m^2 + v_\theta^2)] \tag{7}$$

The source term K_2 arises from the centrifugal force term in the r component of the m momentum equation,

$$K_2 = (\rho v_\theta^2 + p - Re^{-1}\sigma_{22})r_m/r + (p - Re^{-1}\sigma_{33})h_m/h \tag{8}$$

where

$$\frac{r_m}{r} = \frac{1}{r}\frac{dr}{dm}$$

$$\frac{h_m}{h} = \frac{1}{h}\frac{dh}{dm}$$

Although a similar source term arises from the Coriolis force in the θ momentum equation, the equation has been made conservative by multiplying through by r.

The viscous flux term is

$$\hat{S} = \bar{J}^{-1}\begin{bmatrix} 0 \\ S_2 \\ S_3 \\ S_4 \end{bmatrix} \tag{9}$$

where

$$S_2 = \eta_m \sigma_{11} + \bar{\eta}_\theta \sigma_{12}$$

$$S_3 = (\eta_m \sigma_{12} + \bar{\eta}_\theta \sigma_{22})r$$

$$S_4 = \frac{k}{(\gamma - 1)Pr}(\eta_m^2 + \bar{\eta}_\theta^2)\partial_\eta a^2 + v_m S_2 + v_\theta S_3$$

and the shear stress terms are given by

$$\sigma_{11} = 2\mu \partial_m v_m + \lambda \nabla \cdot \bar{V}$$

$$\sigma_{22} = 2\mu(\partial_\theta v_\theta + v_m r_m)/r + \lambda \nabla \cdot \bar{V}$$

$$\sigma_{33} = 2\mu v_m h_m/h + \lambda \nabla \cdot \bar{V}$$

$$\sigma_{12} = \mu[(\partial_m v_\theta - v_\theta r_m/r) + (1/r)\partial_\theta v_m)]$$

$$\lambda \nabla \cdot \bar{V} = -\frac{2}{3}\mu\left[\partial_m v_m + v_m\left(\frac{r_m}{r} + \frac{h_m}{h}\right) + \frac{1}{r}\partial_\theta v_\theta\right] \tag{10}$$

Using the thin-layer approximation, the shear stress terms are evaluated by replacing ∂_m with $\eta_m \partial_\eta$ and $(1/r)\partial_\theta$ with $\bar{\eta}_\theta \partial_\eta$. Here, $a = \sqrt{\gamma p/\rho}$ is the sonic velocity and the normalized thermal conductivity $k = 1$.

The equations are nondimensionalized by arbitrary reference quantities (here the inlet total density and critical sonic velocity define the reference state), and the Reynolds number Re and Prandtl number Pr must be specified in terms of that state. These equations assume that the specific heats C_p and C_v and the Prandtl number are constant, that Stokes' hypothesis $\lambda = -\frac{2}{3}\mu$ is valid, and that the effective viscosity may be written as

$$\mu = \mu_{\text{laminar}} + \mu_{\text{turbulent}}$$

The transformation metrics are found using

$$\begin{pmatrix} \xi_m & \xi_\theta \\ \eta_m & \eta_\theta \end{pmatrix} = J\begin{pmatrix} \theta_\eta & -m_\eta \\ -\theta_\xi & m_\xi \end{pmatrix} \tag{11}$$

where the Jacobian is given by

$$J = (m_\xi \theta_\eta - m_\eta \theta_\xi)^{-1} \tag{12}$$

Overbars in Eqs. (4–9) denote a rescaling of the metrics:

$$\bar{\xi}_\theta = \xi_\theta/r, \quad \bar{\eta}_\theta = \eta_\theta/r, \quad \bar{J}^{-1} = rhJ^{-1} \tag{13}$$

For turbulent flows the two-layer eddy-viscosity model developed by Baldwin and Lomax[9] is used. In the (m, θ) coordinate system the wall shear τ_w and vorticity ω required by the model are given by

$$\tau_w = \sigma_{12w} = \mu\left(\partial_m v_\theta + \frac{1}{r}\partial_\theta v_m - \frac{v_\theta r_m}{r}\right)_w$$

$$\omega = \frac{1}{2}\left(\partial_m v_\theta - \frac{1}{r}\partial_\theta v_m + \frac{v_\theta r_m}{r}\right) \tag{14}$$

The transition model proposed in Ref. 9 was used here. In this model $\mu_{\text{turbulent}}$ is set to zero throughout a profile if the maximum value of $\mu_{\text{turbulent}}/\mu_{\text{laminar}}$ is less than 14.

Computational Grid

Body-fitted C-type grids for this work were generated using the GRAPE code developed by Sorenson.[10,11] Figure 2 shows typical grids around the first-stage stator and rotor of the SSME. The stator grid was modified by adding a single grid line parallel to the exit to allow approximately one cell of overlap with the rotor grid. The rotor grid also was selectively refined by doubling the number of ξ = const grid lines in the inlet region. Both grids were modified by adding one line of dummy points (not shown) corresponding to interior points from neighboring passages. These points are used for imposing the periodic or overlap boundary conditions.

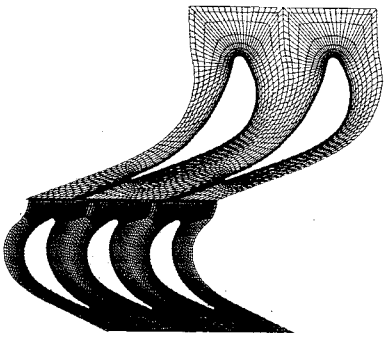

Fig. 2 Computational grids about SSME.

Multistage Runge-Kutta Algorithm

An explicit multistage Runge-Kutta algorithm based on the work of Jameson et al.[12,13] is used to advance the flow equations in time. Given the residual R from a central-difference representation of Eq. (3), a k-stage scheme may be written as follows:

$$q^{(0)} = q^n$$

$$q^{(1)} = q^{(0)} - \alpha_1 \bar{J}\Delta t[Rq^{(0)} - D(q^{(0)})]$$

$$\vdots$$

$$q^{(k)} = q^{(0)} - \alpha_k \bar{J}\Delta t[Rq^{(k-1)} - D(q^{(0)})]$$

$$q^{n+1} = q^{(k)} \tag{15}$$

The time step is given by $\Delta t = \min(\Delta t_{i,j})$, where $\Delta t_{i,j}$ is calculated from an inviscid stability analysis of Eqs. (3–15) to be

$$\Delta t_{i,j} = \frac{CFL}{\left[|v_m|l_m + |w_\theta|l_\theta + a\sqrt{l_m^2 + l_\theta^2} + \dfrac{v_\theta r_m / r}{2a\sqrt{l_m^2 + l_\theta^2}}\right]} \tag{16}$$

where l_m and l_θ are reciprocal length scales given by

$$l_m = |\xi_m| + |\eta_m|$$

$$l_\theta = |\bar{\xi}_\theta| + |\bar{\eta}_\theta| \tag{17}$$

In this work, we have used a four-stage scheme with the standard coefficients $\alpha_i = (\frac{1}{4}, \frac{1}{3}, \frac{1}{2}, 1)$. This scheme is second-order accurate in time and has a Courant limit $CFL = 2.8$. The results shown here were calculated with a maximum Courant number of 2.5, which occurs in fine-grid regions near the wall. Courant numbers in the coarse-grid core flow regions are typically two orders of magnitude smaller for viscous flows.

Artificial Dissipation

Dissipative terms consisting of fourth and second differences are added to prevent odd-even point decoupling and to allow shock capturing, respectively. The dissipative term D in Eq. (15) is given by

$$Dq = (D_\xi + D_\eta)q \tag{18}$$

The ξ-direction operator is given by

$$D_\xi q = C(V_2 q_{\xi\xi} - V_4 q_{\xi\xi\xi\xi}) \tag{19}$$

where

$$C = \frac{1}{\bar{J}\Delta t_{ij}}$$

is a coefficient that partially cancels similar terms in Eq. (15). We have found that using the spatially varying time step Δt_{ij} [Eq. (16)] as a coefficient in the dissipation is much less dissipative than using the minimum time step.

The terms V_2 and V_4 are given by

$$V_2 = \mu_2 \max(\nu_{i+1,j}, \nu_{i,j}, \nu_{i-1,j})$$

$$V_4 = \max(0, \mu_4 - V_2) \tag{20}$$

where

$$\nu_{i,j} = \frac{|p_{i+1,j} - 2p_{i,j} + p_{i-1,j}|}{|p_{i+1,j} + 2p_{i,j} + p_{i-1,j}|} \tag{21}$$

$$\mu_2 = O(1) \tag{22a}$$

$$\mu_4 = O(1/16) \tag{22b}$$

In smooth regions of the flow, the dissipative terms are of third order and thus do not detract from the formal second-order accuracy of the scheme. Near shocks, $\nu_{i,j}$ is large and the second-difference dissipation becomes locally of first order.

Boundary Conditions

Inlet

At the inlet to the stator, total pressure, total temperature T', and the whirl rv_θ are specified. At each time step, the upstream-running Riemann invariant $R^- = v_m - 2a/(\gamma - 1)$ is extrapolated to the inlet. The axial velocity component v_m is found using

$$v_m = \frac{(\gamma - 1)R^- + \sqrt{(\gamma + 1)(4C_pT' - 2v_\theta^2) - 2(\gamma - 1)(R^-)^2}}{(\gamma + 1)} \tag{23}$$

Density and energy are found using isentropic relations. This is a nonreflective approximation to the axial momentum equation that is first-order accurate in space, but zero order in time. However, in the present results, we see virtually no unsteady behavior at the inlet boundary.

Outlet

At the exit from the rotor, static pressure is specified and the other flow quantities are found using second-order extrapolation of ρ, ρv_m, and ρv_θ. The interaction between the specified exit pressure and the inlet conditions sets the mass flow through the machine. This exit condition is strictly reflective and may influence the unsteady solution. We hope to sort out the effects of this condition in future work.

Solid Wall

Blade surface pressures are found from the normal momentum equation,

$$(\xi_m\eta_m + \bar{\xi}_\theta\bar{\eta}_\theta)\partial_\xi p + (\eta_m^2 + \bar{\eta}_\theta^2)\partial_\eta p$$
$$= -\rho W^\xi(\eta_m \partial_\xi v_m + \bar{\eta}_\theta \partial_\xi v_\theta) + \rho v_\theta(\eta_m v_\theta - \bar{\eta}_\theta v_m) r_m/r \tag{24}$$

Surface velocities are found from the tangency or no-slip conditions for inviscid or viscous flows, and the blade temperature is specified.

Periodic Boundaries

The periodic boundaries are solved in the same way as the interior points. The grid for each blade is overlapped one grid cell at its periodic boundary such that the grid points are coincident with the grid points of an adjacent blade. These overlap dummy grid points are updated when an adjacent blade is solved and then are used in the next time-step integration. For equal pitch blade rows, the flow variables on the spatially periodic boundaries are equal on each blade. This is not true for multipassage calculations. Here, periodic boundary conditions are enforced only on boundaries of blades that are encompassed by the blade ratio. Flow variables on interior boundaries are updated using quantities from adjacent blade solutions.

Interface Formulation

For a given displacement between stator and rotor blade rows, the solution on the interface must be determined. Figure

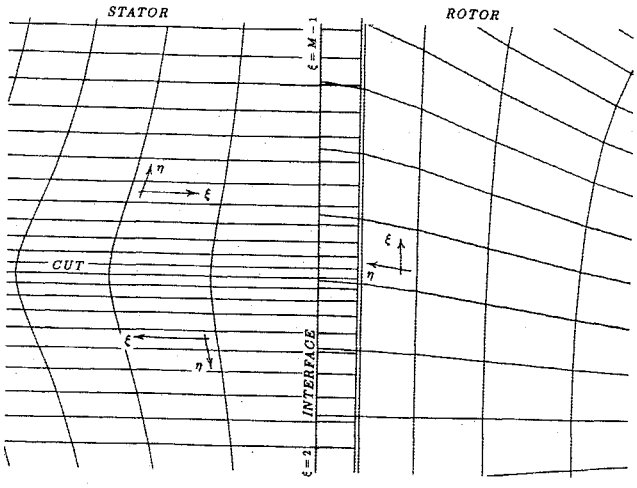

Fig. 3 Enlargement of grid at the interface.

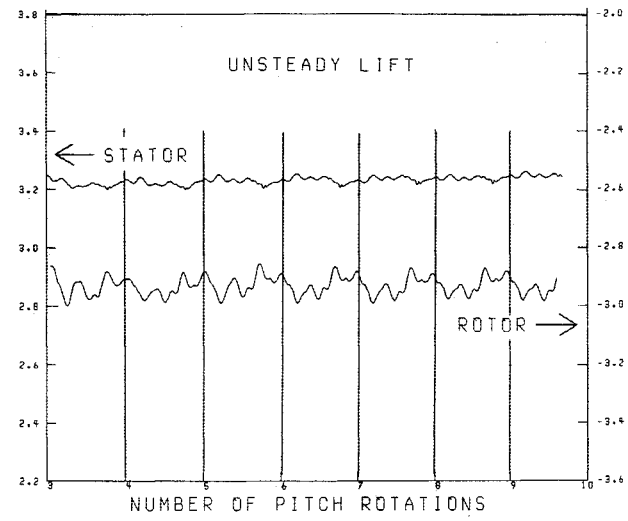

Fig. 4 Unsteady lift diagram for 1:1.

3 shows an enlargement of the interface geometry of the stator and rotor grids. The upstream boundary of the rotor is coincident with the $\xi = 2$ and $\xi = M - 1$ grid lines in the stator grid. The stator grid extends into the rotor grid such that the exit boundary grid points of the stator lie within the first cell of the rotor domain.

The solution is updated at the interface by interpolating the flux variables in the stator computational domain to obtain rotor quantities and interpolating the flux variables in the rotor computational domain to obtain stator quantities. The interface is updated in this way after every Runge-Kutta integration sweep of the stator and rotor domains. Rai[1,2,6] has stressed the importance of conservative treatment of the interface. Our present formulation is nonconservative and the importance is unknown.

Solution Procedure

Initial Conditions

Given a desired leading-edge velocity triangle and exit flow angle for each blade, the initial conditions are calculated using an analytic solution of the one-dimensional flow equations.[7] These initial conditions do not especially speed the convergence to a periodic unsteady solution, but they do provide a smooth transition between the inlet and exit boundary conditions.

Startup

Since the initial conditions are not known, it is desirable to reach the conditions where the initial transcients are no longer in the solution domain. From the initial analytic flow conditions, the solution is integrated using a local time step. This allows the mass flow to stabilize and the wake region to develop quickly. A constant minimum time step then is used to compute the time-accurate solution.

Data Management

In a steady-state analysis, the solution can be converged rapidly by using a local time step and multigrid. When a time-accurate solution is desired, a multigrid procedure cannot be used and a minimum time step must be used in the integration procedure. This is further restricted when rotor/stator interaction is considered, since the solution must be integrated using a constant minimum time step based on the computational domain of two blades.

Our current strategy is to update each blade row a full time step (four Runge-Kutta stages) and then to update the inflow, exit, blade, and interface boundaries. The solution is considered converged when the loading on the blades becomes periodic in time.

The solution for each passage is stored as a separate array in core and accessed as the solver alternates from one blade to the next. The flow solver is relatively unaffected by the number of passages, so that the multipassage problem becomes a problem of data management.

Results

The solution procedure has been applied to the first-stage turbine rotor of the SSME fuel turbopump. The actual SSME stator/rotor blade count ratio for the first stage is 41:63. The numerical procedure was first applied to a single-passage blade row configuration where the stator was scaled to the rotor pitch. The scaling was done such that the pitch-to-chord ratio remained unchanged.

The grids generated using the GRAPE code have viscous spacings of 0.0002 in. away from the blade where the stator axial chord is 1.02 in. and the rotor axial chord is 0.73 in. Both blades have a constant radius of 5.095 in. The stator grid has 115×31 points. The rotor grid has 197×41 grid points. It was necessary to cluster grid points at the inlet of the rotor to get the necessary resolution to capture the wake from the upstream stator. The Reynolds number based on the stator stator axial chord and inlet velocity is 9.25×10^4.

The absolute flow Mach number varies from 0.148 at the stator inlet through about 0.472 between the blade rows to 0.201 at the rotor exit. The inlet absolute flow angle to the stator is 0.0 deg, and the relative inlet flow angle to the rotor is -31.0 deg. Using the above grid spacing, flow conditions, and a maximum Courant number of 2.5, the time step is calculated based on the inviscid stability limit for the four-stage Runge-Kutta scheme. The time step is such that it takes 11,262 steps to move one rotor pitch. This takes about 18 min on the Cray X-MP for the equal pitch computation. A solution is considered converged when the unsteady lift on each blade becomes periodic. For the equal passage machine, this convergence criterion is met after seven rotor blade passings. This requires 2.10 h of computer time.

The unsteady lift diagrams for the single passage machine are shown in Fig. 4. Fluctuations in lift on the stator are minimal but are more dramatic on the rotor. The minimum lift takes place when the rotor begins to pass through the wake of the stator.

The static pressure envelope for the stator (Fig. 5) indicates that the only influence of the downstream rotor is on the uncovered portion of the suction surface of the stator. The major portion of the blade remains unchanged from the time-averaged solution. The static pressure envelope of the rotor (Fig. 6) shows a larger influence of the stator wake at the leading edge of the rotor blade, which influences the rest of the blade. Slight discontinuities in the pressure distribution

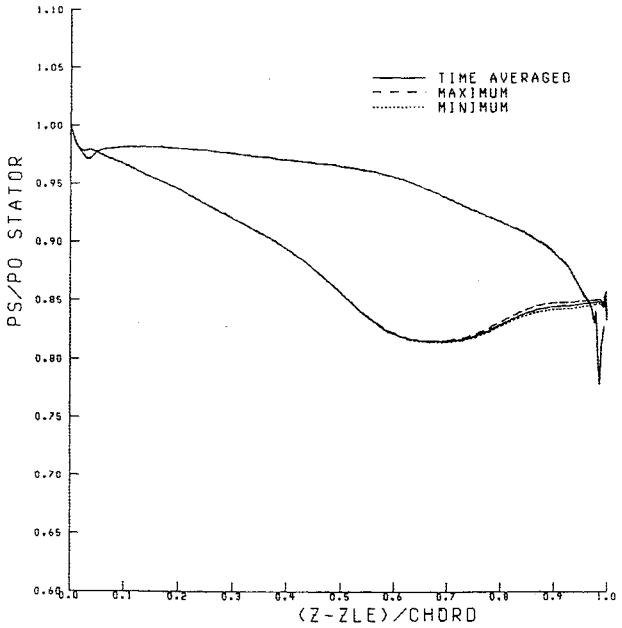

Fig. 5 Static pressure envelope on stator (1:1, viscous).

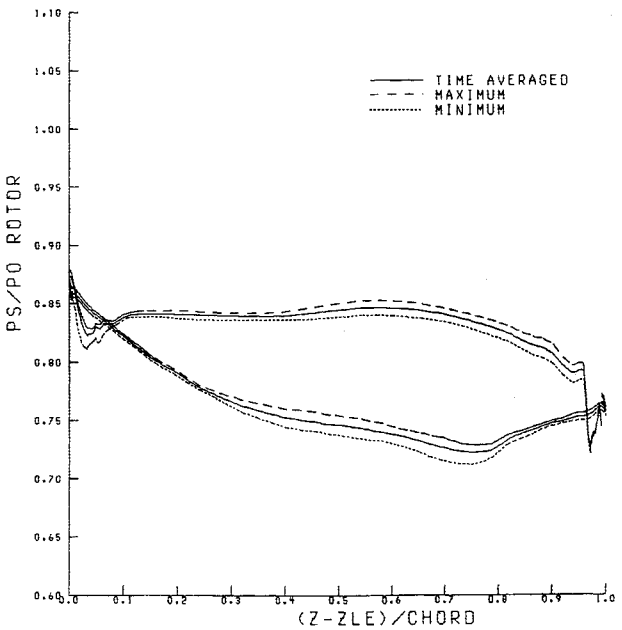

Fig. 6 Static pressure envelope on rotor (1:1, viscous).

near 1% chord on the suction surface and 5% chord on the pressure surface are due to abrupt discontinuities in surface curvatures where the round leading edge meets the blade surfaces. The adverse pressure gradient seen on the pressure surface is caused by the leading-edge geometry and the low incidence angle of the flow. This adverse gradient causes the flow to separate from the pressure surface as a classic cove separation, with reattachment well downstream as seen in Fig. 7. The cove separation disappears at higher incidence angles.

Figures 8 and 9 show Mach contours as the rotor moves through the stator wakes. Remnants of the wakes from other stator blades can be seen in the rotor passage. When entropy contours are plotted in Fig. 10, this is more apparent.

Next, we present results for a multipassage configuration with a 2:3 blade count that is close to that of the actual machine. The unsteady lift diagrams are shown in Fig. 11 for a single stator and a single rotor. The effect of the larger upstream stators on the downstream rotors is much more dramatic than seen in the single-passage computation. Again,

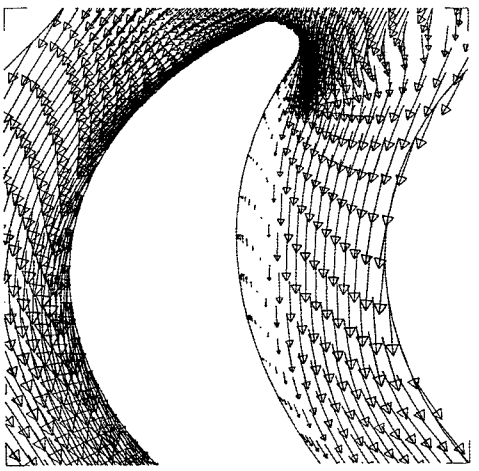

Fig. 7 Relative velocity vectors on rotor showing cove separation (1:1).

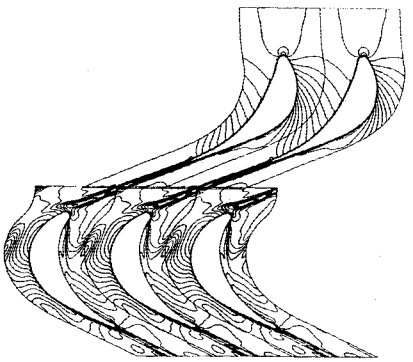

Fig. 8 Mach number contours (1:1, ½ pitch rotation).

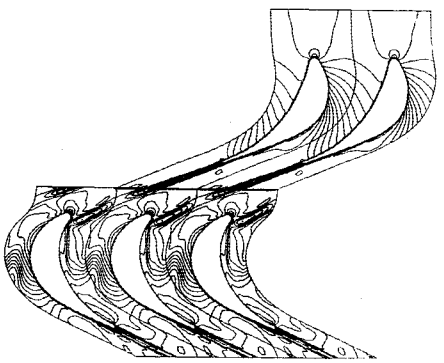

Fig. 9 Mach number contours (1:1, aligned).

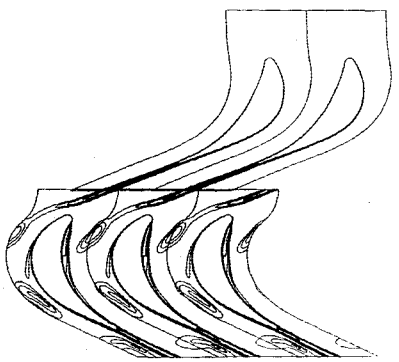

Fig. 10 Entropy contours (1:1).

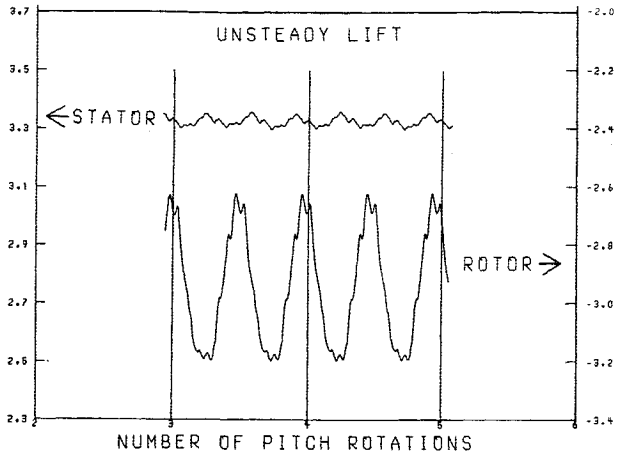

Fig. 11 Unsteady lift (2:3, viscous).

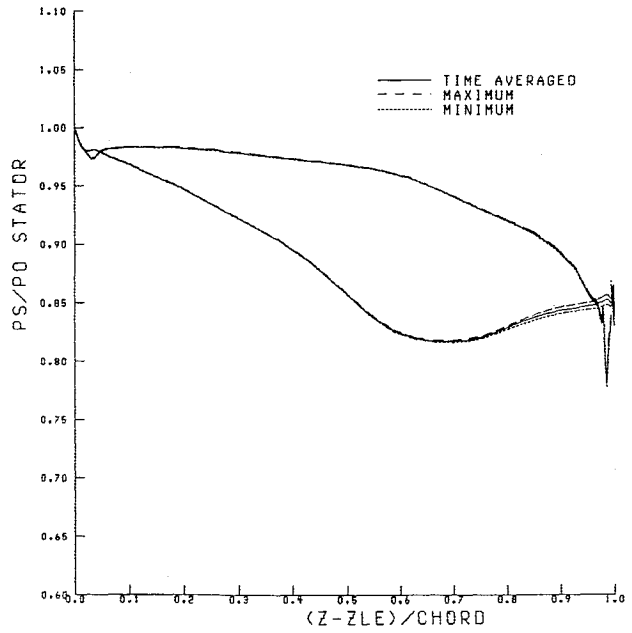

Fig. 12 Static pressure envelope on stator (2:3).

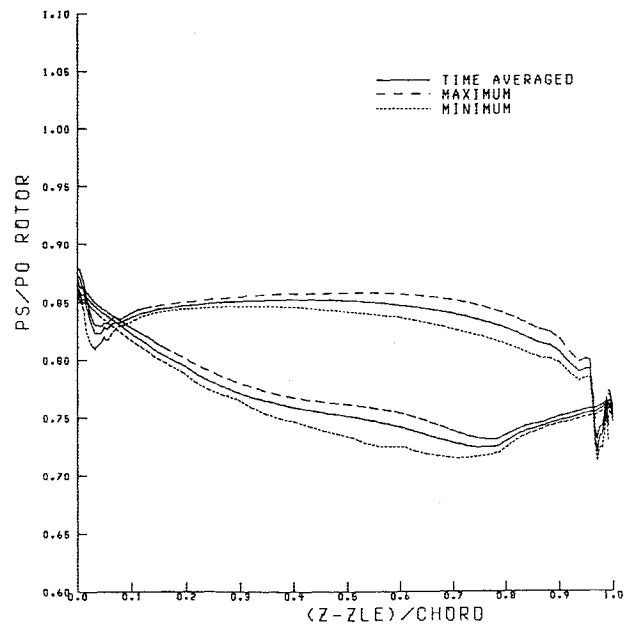

Fig. 13 Static pressure envelope on rotor (2:3).

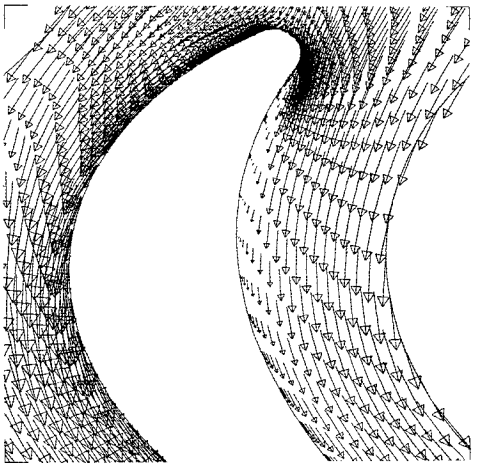

Fig. 14 Relative velocity vectors on rotor showing cove separation (2:3).

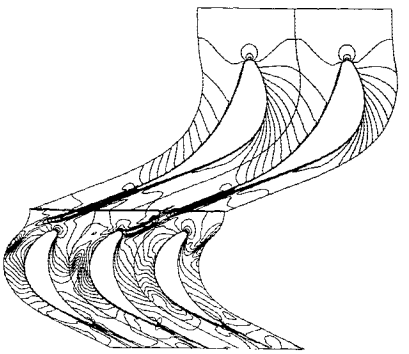

Fig. 15 Mach number contours (2:3, aligned).

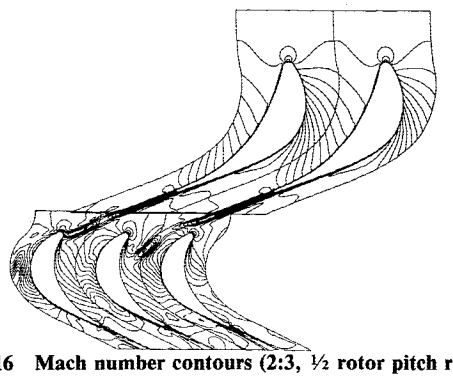

Fig. 16 Mach number contours (2:3, ½ rotor pitch rotation).

the stator row sees only small fluctuations due to the rotor passing by downstream. The three fluctuations seen in the lift show the influence of the three passing downstream rotors over a periodic pitch. A rotor passes through two stator wakes over one periodic pitch rotation. The rotor sees large fluctuations in its lift, with the minimum lift occurring when the rotor's leading edge encounters the wake of the upstream stator. A periodic solution is obtained after about seven rotor blade passings. This takes about 6 h of computer time and requires about 1.25 times the storage of a single-passage computation.

The static pressure envelope for the multipassage stator (Fig. 12) shows the fluctuation in the pressure only on the uncovered portion of the suction surface of the blade. The pressure gradient is less adverse than that seen on the single-passage machine. The static pressure envelope on the rotor (Fig. 13) shows a larger static pressure fluctuation along the entire surface of the blade. The adverse pressure gradient seen on the pressure surface near the leading edge generates a smaller cove separation on the multipassage machine (Fig. 14).

Figures 15 and 16 show Mach contours for the multipassage machine. The asymmetry of the flow is apparent in the rotor

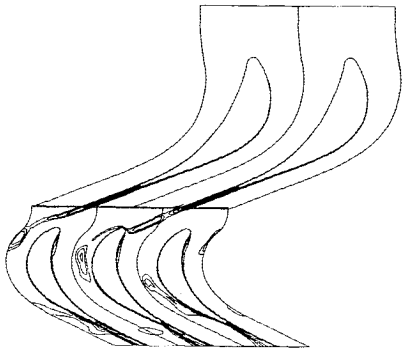

Fig. 17 Entropy contours (2:3).

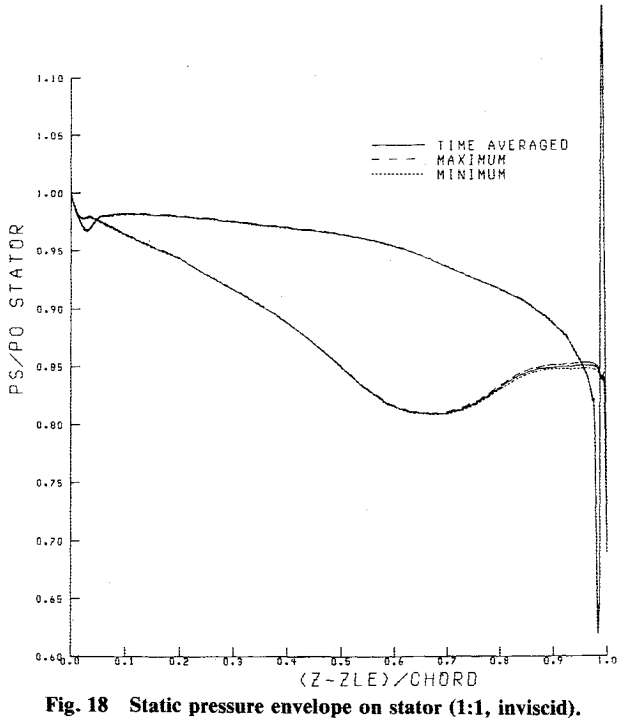

Fig. 18 Static pressure envelope on stator (1:1, inviscid).

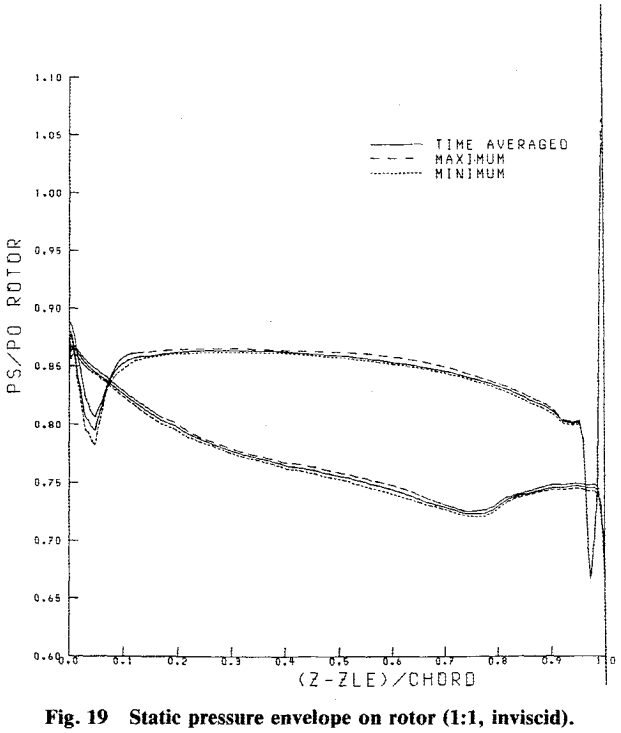

Fig. 19 Static pressure envelope on rotor (1:1, inviscid).

passages. Here, the stator wakes can be seen at different locations of rotation. Again, the entropy contours (Fig. 17) clearly show the asymmetry of the different rotor passages as the wakes move downstream.

The inviscid solution of a single-passage machine was computed by matching the static pressure at the exit of the rotor with that of the viscous solution. The grids used in this calculation allowed a larger time step to be used such that 1874 iterations were necessary to move one pitch rotation.

The static pressure envelope on the stator (Fig. 18) shows fluctuations similar to those in the viscous computations. On the rotor (Fig. 19), the static pressure plots show a larger adverse pressure gradient at the leading edge and a faster recovery. Also, the fluctuations in pressure along the rotor blade due to the upstream stator in the viscous solution are not as prominent in the inviscid solution.

Conclusions

The quasi-three-dimensional Euler or the thin-layer Navier-Stokes equations are solved for unsteady turbomachinery flows. These equations are written in general coordinates for an axisymmetric stream surface and account for the effects of blade row rotation, radius change, and stream surface thickness.

A four-stage Runge-Kutta scheme based on the work of Jameson is used to predict time-accurate results. A nonconservative interface formulation and other data management techniques allow the solution of rotor/stator interaction problems in both single- and multipassage machines.

Viscous results on the first stage of the Space Shuttle main engine high-pressure fuel turbopump have shown the analysis to be viable. Results have been shown on the scaled single- as well as the multipassage machine. The fact that the analysis is quasi-three-dimensional will allow the time-accurate solution of radial flow turbomachinery.

References

[1]Rai, M. M., "A Relaxation Approach to Patched-Grid Calculations with the Euler Equations," AIAA Paper 85-0295, Jan. 1985.

[2]Rai, M. M., "Navier-Stokes Simulations of Rotor-Stator Interaction Using Patched and Overlaid Grids," AIAA Paper 85-1519, July 1985.

[3]Gibeling, H. J., Weinberg, B. C., Shamroth, S. J., and McDonald, H., "Flow Through a Compressor Stage," Scientific Research Associates, Inc., Glastonbury, CT, Air Force Office of Scientific Research, R86-910004-F, May 1986.

[4]Oden, J. T. and Bass, J. M., "Adaptive Computational Methods for Fluid-Structure Interaction in Internal Flow," Computational Mechanics Co., Austin, TX, Phase I Report for NASA SBIR Contract NAS3-24849, Sept. 1986.

[5]Giles, M., "Calculation of Unsteady Wake/Rotor Interactions," AIAA Paper 87-0006, Jan. 1987.

[6]Rai, M. M., "Unsteady Three Dimensional Navier-Stokes Simulations of Turbine Rotor-Stator Interaction," AIAA Paper 87-2058, June 1987.

[7]Chima, R. V., "Explicit Multigrid Algorithm for Quasi-Three-Dimensional Viscous Flows in Turbomachinery," *Journal of Propulsion and Power,* Vol. 3, Sept.-Oct. 1987, pp. 397-405.

[8]Chima, R. V., "Inviscid and Viscous Flows in Cascades with an Explicit Multiple-Grid Algorithm," *AIAA Journal,* Vol. 23, Oct. 1985, pp. 1556-1563.

[9]Baldwin, B. S. and Lomax, H., "Thin-Layer Approximation and Algebraic Model for Separated Turbulent Flows," AIAA Paper 78-257, Jan. 1978.

[10]Sorenson, R. L., "A Computer Program to Generate Two-Dimensional Grids About Airfoils and Other Shapes by the Use of Poisson's Equation," NASA TM-81198, May 1980.

[11]Steger, J. L. and Sorenson, R. L., "Automatic Mesh-Point Clustering Near a Boundary in Grid Generation with Elliptic Partial Differential Equations," *Journal of Computational Physics,* Vol. 33, No. 3, Dec. 1979, pp. 405-410.

[12]Jameson, A., Schmidt, W., and Turkel, E., "Numerical Solutions of the Euler Equations by Finite Volume Methods Using Runge-Kutta Time-Stepping Schemes," AIAA Paper 81-1259, June 1981.

[13]Jameson, A. and Baker, T. J., "Solution of the Euler Equations for Complex Configurations," AIAA Paper 83-1929, July 1983.